Journal of
Composites Science

MDPI

Article

Black Phosphorus-Based ZnO-Ag Nanocomposite for Antibacterial Activity against Tigecycline-Resistant *Acinetobacter baumannii*

Atanu Naskar, Hyejin Cho and Kwang-sun Kim *

Department of Chemistry and Chemistry Institute for Functional Materials, Pusan National University, Busan 46241, Republic of Korea; atanunaskar@pusan.ac.kr or atanunaskar22@gmail.com (A.N.); chj9512@pusan.ac.kr (H.C.)
* Correspondence: kwangsun.kim@pusan.ac.kr; Tel.: +82-51-510-2241

Abstract: *Acinetobacter baumannii* is a critically hard-to-treat gram-negative pathogen responsible for a range of infectious diseases. Tigecycline is a last-resort antibiotic for *A. baumannii* infection; however, tigecycline-resistant (TIG-R) *A. baumannii* has been increasingly reported. Therefore, new strategies must be developed to treat these detrimental infections. Nanoantibiotics composed of two-dimensional (2D) black phosphorus (BP) and its derived nanocomposites have emerged as excellent alternatives to current antibiotics. However, the development of unique materials to target specific pathogens is challenging. Here, we report the preparation of a BP-based ZnO-Ag (ZPBA) nanocomposite. A low-temperature solution synthesis method was used to prepare ZnO and Ag nanoparticles immobilized on BP nanosheets. X-ray diffraction, transmission electron microscopy, and X-ray photoelectron spectroscopy were used to characterize the ZPBA nanocomposite. The antibacterial activity of ZPBA nanocomposite was assessed by determining its minimum inhibitory concentration against type (ATCC 19606, ATCC 15150) and TIG-R (ATCC 19606-R) *A. baumannii* strains. From the assays, ZPBA showed superior activity against TIG-R *A. baumannii* strain with MIC of 12.5 $\mu g \cdot mL^{-1}$ compared to all other prepared samples. Finally, the combination of bacterial membrane disruption and ROS generation was demonstrated to be a potential antibacterial mechanism of ZPBA. Our results show that ZPBA could be a potential nanoantibiotic platform for eradicating TIG-R *A. baumannii.*

Keywords: black phosphorus; nanocomposite; tigecycline-resistant *Acinetobacter baumannii*; gram-negative bacteria; antibacterial

check for updates

Citation: Naskar, A.; Cho, H.; Kim, K.-s. Black Phosphorus-Based ZnO-Ag Nanocomposite for Antibacterial Activity against Tigecycline-Resistant *Acinetobacter baumannii*. *J. Compos. Sci.* **2023**, *7*, 423. https://doi.org/10.3390/jcs7100423

Academic Editor: Francesco Tornabene

Received: 30 August 2023
Revised: 7 October 2023
Accepted: 8 October 2023
Published: 9 October 2023

1. Introduction

Acinetobacter baumannii is a problematic nosocomial gram-negative pathogen involved in multiple infectious diseases, such as pneumonia [1], and is classified by the World Health Organization (WHO) as a critical priority list for research and development of bacteria to request immediate consideration for the discovery of new class antibiotics or alternatives to antibiotics [2]. Owing to its intrinsic resistance to antibiotic therapies and the easy acquisition of new resistance mechanisms, multidrug-resistant (MDR) *A. baumannii* is prevalent in all *A. baumannii* populations [1]. It is worthy to note that the estimated global incidence of infections related to *A. baumannii* is approximately one million cases annually [3]. Moreover, it is one of the most resistant organisms encountered in clinical practice [4]. Hospitalized patients, especially those in the intensive care unit (ICU), are at a higher risk of *A. baumannii* infections. However, *A. baumannii* is difficult to remove from the environment, causing deadly infections and large outbreaks among hospitalized patients and nursing home residents. There are only a few options for treating infections caused by MDR *A. baumannii*, including tigecycline (TIG), the first member of the glycylcycline class antibiotics derived from tetracyline [5] and a last-resort antibiotic against *A. baumannii* [6].

However, the prevalence of TIG-R *A. baumannii* has also been rapidly increasing [7]. Since the increasing rate of TIG-R *A. baumannii* has become a significant burden on the healthcare system and the rapid decline in the current arsenal of effective antibiotics, it is necessary to find alternatives to antibiotics against TIG-R *A. baumannii* infections.

In this regard, new-generation nanomaterials show excellent potential against drug-resistant bacterial pathogens owing to their unique physiochemical characteristics and can be an alternative to antibiotics [8]. It is well known that the mechanism of nanomaterials is quite different that from of antibiotics, and direct contact with cell membranes without penetrating the cells prevents bacterial resistance against them [9]. In the present scenario, various 2D nanomaterials [10], especially black phosphorus (BP), have shown excellent potential for antibacterial applications [11]. Similar to graphene, BP nanosheets (NSs) can slash the bacterial membrane owing to the presence of sharp edges and large surface-to-volume ratio, which can ultimately kill bacterial cells [12]. Additionally, it can form nanocomposites with other antibacterial nanomaterials composed of metals (e.g., Ag and Au) and metal oxides (e.g., ZnO) for synergistic and more effective antibacterial activity than individual nanomaterials [13,14]. In fact, the structure of BP is not flat in a strict sense and consists of a lone-pair electron on the outside which enables them with an effective interfacial charge transfer activity and makes it an excellent candidate for the preparation of metal-based nanocomposites with improved activity [15]. Notably, BP can also act as a green resuctant to produce Ag or Au nanoparticles (NPs) without any surfactant intervention [13].

In addition to the new-generation nanomaterials, the antibacterial potential of inorganic nanomaterials such as ZnO, CuO, Fe_2O_3, Ag, Au, antimicrobial nanostructured coatings and CuS, is already reported by many research works [16–18]. Moreover, stability, broad-spectrum antibacterial activity and low drug resistance are some of the advantages, which can be assigned to inorganic nanomaterials. ZnO nanomaterial has shown immense potential for antibacterial activity against various pathogens due to its favorable physicochemical properties [13,14]. Moreover, there is no argument regarding the potential antibacterial activity of Ag NPs. The antibacterial activity of Ag NPs depends on the amount of Ag^+ released, which is achieved using different sizes, shapes and surface coatings [19]. However, the overuse of Ag NPs can cause gastrointestinal disorders, spasms and even death in humans [20]. Moreover, bare Ag NPs tend to aggregate upon contact with bacteria, which sometimes hinders their activity [21]. Therefore, it is appropriate to develop nanocomposites in which the activity of Ag NPs can be properly controlled and optimized. Hence, the combination of BP and Ag NP along with ZnO NP can pave the way for an excellent nanocomposite, where the synergistic activity and selective pressure of the nanocomposite is greater than that of individual activity in eradicating bacterial infections.

Another aspect of Ag NPs, which is worth utilizing in the development of new antibacterial agents, is that they are more selective against gram-negative bacteria than gram-positive bacteria [22,23] owing to the structural differences in bacterial cells. Compared to gram-positive bacteria, gram-negative bacteria have a thinner peptidoglycan layer, which enhances the chance of Ag NP penetration into bacteria and subsequent bacterial killing. Moreover, there are many works regarding the antibacterial activity based on Ag-ZnO [24], ZnO-BP [25], or BP [11] itself. However, ZnO-, Ag- and BP-based nanocomposites have not been utilized for antibacterial activity.

Different methods [26] have been utilized for the synthesis of NPs, such as sol-gel, hydrothermal, laser ablation and microemulsion methods. However, the requirements of high energy consumption, high pressure–temperature complexity, environmental impact, lengthy production time, and obviously low production remain some of the drawbacks associated with them. In this regard, low-temperature solution synthesis of metals (e.g., Ag), or metal oxides (e.g., ZnO) synthesis has garnered considerable interest due to its simplicity and large-scale production at a low cost [27–29].

Based on the above considerations, an Ag NP and ZnO-loaded BP (ZPBA) nanocomposite was synthesized and its antibacterial potential against *A. baumannii* was evaluated.

Initially, a low-temperature solution process was used to synthesize ZnO NP. Subsequently, ZnO and Ag NPs were immobilized onto BP NSs without the use of any surfactant. The material properties of the samples were characterized to confirm the nanocomposite formation. Furthermore, the antibacterial activity of ZPBA nanocomposite against type and TIG-R *A. baumannii* strains was assessed, and it was found that ZPBA showed better activity and selectivity compared to nanocomposites composed of BP-Ag (BA), ZnO-PEG (ZP), ZP-Ag (ZPA), or ZP-BP (ZPB) to TIG-R *A. baumannii*. All our results indicate that both Ag NP and BP can synergize the antibacterial activity of ZnO NP with better efficacy against TIG-R *A. baumannii*. Therefore, our newly synthesized nanocomposite could serve as a potential platform against TIG-R *A. baumannii* infections.

2. Experimental

2.1. Synthesis of ZnO-PEG (ZP) NPs

ZP NPs were successfully synthesized using protocols of previous work with a slight modification [13]. At first, 50 mL of 0.2 M aqueous solution of zinc nitrate hexahydrate [$Zn(NO_3)_2 \cdot 6H_2O$, 98%, Sigma-Aldrich, St. Louis, MO, USA] was prepared by continuous stirring for 15 min at 25 °C. Subsequently, 2 g of polyethylene glycol (PEG) with an average mol wt. 8000 (Sigma-Aldrich, St. Louis, MO, USA) was added to the solution under continuous stirring. The 50 mL of 1.6 M sodium hydroxide (NaOH, 95%, Junsei, Tokyo, Japan) aqueous solution was prepared in another beaker. At this point, the prepared NaOH solution was added dropwise to $Zn(NO_3)_2$ with the PEG reaction mixture under continuous stirring to obtain a white precipitate on the bottom of the beaker. Subsequently, the mixture was stirred at 80 °C for 6 h. The mixture was then immediately transferred immediately to an ice bath to stop the reaction. Finally, the white precipitate obtained was collected after centrifugation with deionized water (DW) and ethanol and dried in an air oven at 60 °C overnight.

2.2. Syntheses of BP, NS and BP-Based Nanocomposites

2.2.1. Synthesis of BP NS

A previously developed method was utilized for the synthesis of BP NS from bulk BP crystals [30]. Initially, 2.0 g of NaOH was added to 60 mL of N-methyl-2-pyrrolidone (NMP; Sigma-Aldrich, St. Louis, MO, USA) and sonicated in a water bath for 5 min. The supernatant was collected via centrifugation. Later, 25 mg of bulk BP crystals were added to the NMP-containing saturated NaOH solution, for an ice bath ultrasonication for 8 h. The bath temperature was maintained at below 20 °C. Subsequently, the unexfoliated BP crystals were removed by centrifuging the dispersion at 2000 rpm for 15 min after completion of the exfoliation step. Finally, the BP NS were collected from the supernatant after centrifugation at 13,000 rpm for 10 min. The BP NS produced were dispersed in DW and stored at 4 °C until further use.

2.2.2. Synthesis of ZP-BP(ZPB) and ZPB-Ag (ZPBA) Nanocomposites

First, 100 mg of as-synthesized ZP was dispersed in 30 mL of DW and ultrasonicated for 10 min. Then, 10.0 mL of aqueous 0.2 M silver nitrate ($AgNO_3$, ≥99.9%; Sigma-Aldrich, St. Louis, MO, USA) was gradually added to the ZP dispersion. Subsequently, the prepared BP NS (4 mL of 2 $mg \cdot mL^{-1}$ concentration) was added. The obtained mixture was ultrasonicated for 10 min followed by continuous stirring for 4 h. ZPBA nanocomposite was collected by centrifugation after the reaction. Finally, the samples were dried in a vacuum oven at 60 °C for 6 h. No surfactant was used for the formation of Ag NP, as BP itself acts as a green reductant during this process. ZPB nanocomposite was synthesized following a similar process, except for the use of silver nitrate. To compare the antibacterial activity, a BP-Ag (BA) nanocomposite was synthesized without the addition of any surfactant and ZnO NP.

2.3. Synthesis of ZP-Ag (ZPA) Nanocomposite

ZPA nanocomposite was synthesized by a surfactant-assisted process following the published protocol without any addition of BP [31]. Briefly, 100 mg of synthesized ZP in 30 mL of DW and 10 mL of an aqueous solution of 0.2 M $AgNO_3$ (≥99.9%, Sigma-Aldrich, St. Louis, MO, USA) were mixed together for 10 min of ultrasonication and stirred continuously. Next, 100 mg of polyvinylpyrrolidone (PVP-40000, Sigma-Aldrich, St. Louis, MO, USA) was added to the dispersion and stirred continuously for 1 h. Subsequently, 0.01 g of $NaBH_4$ and 250 µL of 25% (v/v) NH_3 were mixed in a separate beaker, followed by the addition of 5 mL DW. Subsequently, 2 mL of $NaBH_4$ solution was added to the ZP dispersion under continuous stirring and maintained for 1 h at 25 °C. Finally, the ZPA nanocomposite was collected by centrifugation and air oven-drying at 60 °C overnight.

2.4. Characterization

2.4.1. Material Properties

X-ray diffraction (XRD) characterization was performed to determine the diffraction patterns of samples. An X-ray diffractometer (D8 Advance with a DAVINCI design X-ray diffraction unit, Bruker, Berlin, Germany) with a nickel-filtered Cu K_α radiation source (λ = 1.5406 Å) in the 2θ range of 5–80° was used. For the microstructural analysis of ZPBA nanocomposites, transmission electron microscopy (TEM; Bruker Nano GmbH, Berlin, Germany) was employed using carbon-coated 300-mesh Cu grids. Additionally, the ZPBA nanocomposite was evaluated using an AXIS Supra X-ray photoelectron spectroscopy (XPS) microprobe surface analysis system with a binding energy range of 200–1200 eV to determine the chemical state of elements. The position of the C 1s peak position at 284.5 eV was used as the binding energy reference.

2.4.2. Preparation of Bacterial Cells

In vitro antibacterial activity and morphological characterization against *Acinetobacter baumannii* (ATCC 19606, ATCC 15150) from American Type Culture Collection [ATCC, Manassas, VA, USA; www.atcc.org (accessed on 1 October 2023)] and TIG-R *A. Baumannii* (ATCC 19606-R) [32] were performed. Initially, freshly cultured bacterial colonies from individual strains were obtained using cultures on Luria–Bertani (LB) agar plates. Next, the colonies were resuspended in DW to a McFarland turbidity of 0.5, using a Sensititre™ Nephelometer (Thermo Fisher Scientific, Waltham, MA, USA). The cell suspensions were inoculated into BBL™ Mueller Hinton broth (BD Biosciences, Franklin Lakes, NJ, USA) at a 1000-fold dilution. In the next step, various ZnO-based nanocomposites with different concentrations were added to the cell suspensions, which were then cultured at 37 °C for 16 h. The prepared cell cultures were used for subsequent analysis.

2.4.3. Determination of Minimum Inhibitory Concentration (MIC)

To determine the MICs of nanocomposites, a 96-well-based method from a previous study was used, with a minor modification [33]. Briefly, ATCC 19606, ATCC 15150, and ATCC 19606-R cultures were prepared as described in Section 2.4.2, mixed with different concentrations of BA, ZP, ZPB, ZPA and ZPBA nanocomposites. The mixtures (50 µL) were then incubated at 37 °C for 16 h. The 96-well plates were imaged using a digital camera (Samsung NX200, Suwon, Republic of Korea) for MIC determination. The concentrations of nanocomposites with no visible growth of individual samples were determined as MICs from triplicate experiments.

2.4.4. Morphological Characterization of Bacteria

To investigate the antibacterial mechanism of ZPBA nanocomposite, the morphology of *A. baumannii* (ATCC 19606) cells was examined using the cell suspension treated by ZPBA at a sublethal concentration (a half MIC) as described in Section 2.4.2. The cell pellets from the cultures were collected by centrifugation at 12,000 rpm for 1 min and then resuspended in 500 µL of phosphate-buffered saline (PBS, pH 7) containing 2% formalde-

hyde and 1% glutaraldehyde. The cells were fixed by incubating the mixtures for 5 min at 25 °C. Subsequently, the fixed cells were obtained by centrifugation, washed twice with DW, and resuspended in 1 mL of DW. A silicon wafer (5 × 5 mm, Namkang Hi-Tech Co., Ltd., Seongnam, Republic of Korea) was utilized for deposition, where a 5 μL aliquot from the suspension was deposited and allowed to dry at 25 °C. VEGA3, a versatile tungsten thermionic emission scanning electron microscopy (SEM) system (TESCAN, Fuveau, France) was used to analyze the dried wafer according to the manufacturer's protocol.

2.4.5. Measurement of ROS Production

The ROS production capacity of all the samples against TIG-R was evaluated based on the previous report [17]. Firstly, bacterial cells of 0.5 McFarland turbidity in PBS were treated with ZP, ZPB, ZPA and ZPBA samples at 12.5 $\mu g \cdot mL^{-1}$ in the presence of 2′,7′-dichlorodihydrofluorescin diacetate (DCFH-DA) (Sigma-Aldrich, Burlington, MA, USA) at a final concentration of 30 μM in PBS. After that, the bacterial cell cultures were incubated at 37 °C for 2 h with vigorous shaking (500 rpm). Then, the FLUOstar Omega (BMG Labtech, Ortenberg, Germany) was utilized to measure the amount of ROS based on fluorescence intensity with excitation and emission wavelengths of 485 and 520 nm, respectively. Obviously, the bacterial cell suspension in PBS without any nanoparticle treatment was used as a control. MARS Data Analysis software (ver. 3.02 R2, BMG Labtech, Ortenberg, Germany) was used to further analyze the samples. Triplicate measurements were taken, and the relative ROS production of treated samples was compared to the control; the averaged values with standard deviation ($p < 0.05$) are shown.

3. Results and Discussion

3.1. Material Properties

3.1.1. Phase Structure

XRD characterization was used to analyze the crystalline phases of the synthesized ZP, ZPB and ZPBA samples, as depicted in Figure 1. The XRD patterns of all samples show diffraction peaks consistent with the hexagonal ZO (h-ZnO) structure (JCPDS 36-1451) [33]. In addition, one extra peak was detected at ~16.90° in the enlarged spectra of the ZPB and ZPBA samples, confirming the presence of BP because it corresponds well to the (020) lattice plane of BP [13]. Furthermore, some additional peaks were observed at approximately 38.1°, 44.3°, 64.5° and 77.3° for the ZPBA sample, which corresponds to the crystal planes of cubic Ag (JCPDS 04–0783) along (111), (200), (220) and (311), respectively [31]. The successful formation of Ag NPs without the addition of any surfactants confirmed the green reduction potential of BP. Similarly, cubic Ag NP peaks and h-ZnO peaks were clearly visible for the ZPA sample (Figure S1) where surfactant was used to synthesize Ag NP instead of BP. This ZPA synthesis was implemented to compare the antibacterial activity of the ZPBA sample (where ZnO, BP and Ag were present) with the ZPA sample (where ZnO and Ag are present). Therefore, XRD characterization successfully confirmed the formation of the ZP, ZPB and ZPBA samples.

3.1.2. Morphology and Microstructure

TEM characterization was used to define the morphology of the synthesized ZPBA nanocomposite, as illustrated in Figure 2. TEM images of the ZPBA nanocomposite are depicted in Figure 2a,b, where the distribution of NPs on the surface of the BP nanosheets can be clearly seen. Additionally, the high-resolution TEM (HRTEM; Figure 2c) image of the synthesized ZPBA nanocomposite confirms the formation of ZnO and Ag NPs owing to the existence of distinct lattice fringes with interplanar distances of 0.23 and 0.28 nm correspond to the (111) plane of Ag and the (100) plane of ZnO NPs [31], respectively. Therefore, the TEM and HRTEM results confirmed the successful formation of the ZPBA nanocomposite, which further supported the XRD result (Figure 1). Furthermore, the elemental mapping images of the ZPBA nanocomposite demonstrate good distributions

of the whole (Figure 2d), Zn (Figure 2e), O (Figure 2f), Ag (Figure 2g) and P (Figure 2h) elements.

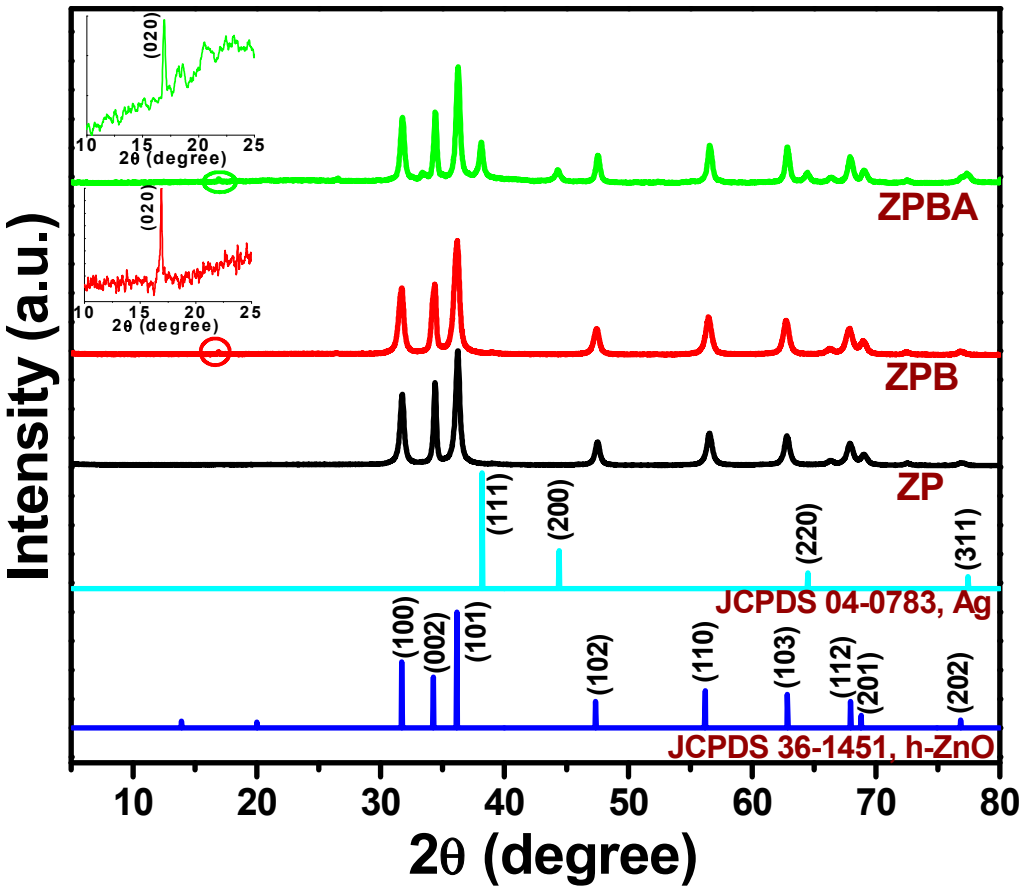

Figure 1. XRD patterns of ZP, ZPB and ZPBA samples. Insets illustrate the enlarged regions in the ZPB and ZPBA spectra marked by circles.

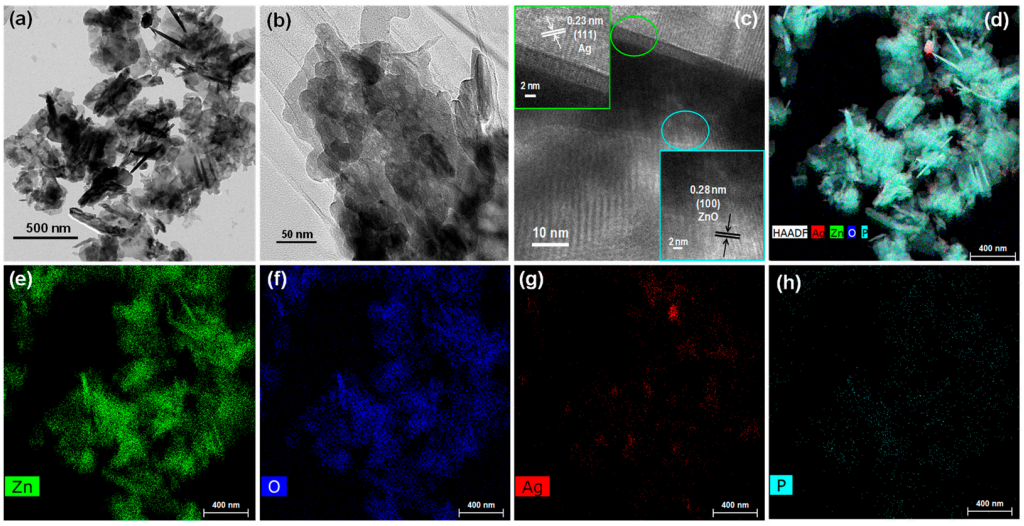

Figure 2. (**a**,**b**) Transmission electron microscopy (TEM) images and (**c**) high-resolution TEM image of the ZPBA nanocomposite with elemental mappings of (**d**) nanocomposite, (**e**) Zn, (**f**) O, (**g**) Ag, and (**h**) P.

3.1.3. XPS Results

XPS characterization was performed on a representative ZPBA nanocomposite to analyze the chemical composition and oxidation state of the chemical elements present in the sample. Figure 3 shows the XPS results of the ZPBA nanocomposite, which confirm the presence of Zn 2p (Figure 3a), Ag 3d (Figure 3b) and P 2p (Figure 3c). Gaussian-fitted component analysis of Zn 2p showed two strong peaks at ~1021.7 eV and ~1044.7 eV (Figure 3a), which corresponded to the binding energy values of Zn $2p_{3/2}$ and Zn $2p_{1/2}$, respectively [31,34–37]. Notably, the difference between these two peaks (~23.0 eV) also confirms the presence of Zn^{2+} in the ZPBA sample, which is in agreement with other studies [13]. Other details including area (Zn $2p_{3/2}$: 55,721; Zn $2p_{1/2}$: 29,914), width (Zn $2p_{3/2}$: 1.5619; Zn $2p_{1/2}$: 1.8109), and height (Zn $2p_{3/2}$: 28,465; Zn $2p_{1/2}$: 13,180) were characterized. An additional Gaussian-fitted process was applied to Ag 3d peaks and identified two strong peaks at 367.5 and 373.5 eV (Figure 3b), which corresponded to Ag $3d_{5/2}$ and Ag $3d_{3/2}$, respectively based on binding energy values [31,37–40], confirming the formation of Ag NPs in ZPBA nanocomposite. Details such as area (Ag $3d_{5/2}$: 2075.1; Ag $3d_{3/2}$: 1443.7), width (Ag $3d_{5/2}$: 0.81835; Ag $3d_{3/2}$: 0.83730) and height (Ag $3d_{5/2}$: 2023.2; Ag $3d_{3/2}$: 1375.8) were also characterized. The presence of BP was confirmed by the presence of P *2p* (Figure 3c) in the nanocomposite [13]. Hence, the successful formation of ZPBA nanocomposite can be easily confirmed by analyzing the chemical composition and valence states of the elements present in ZPBA nanocomposite.

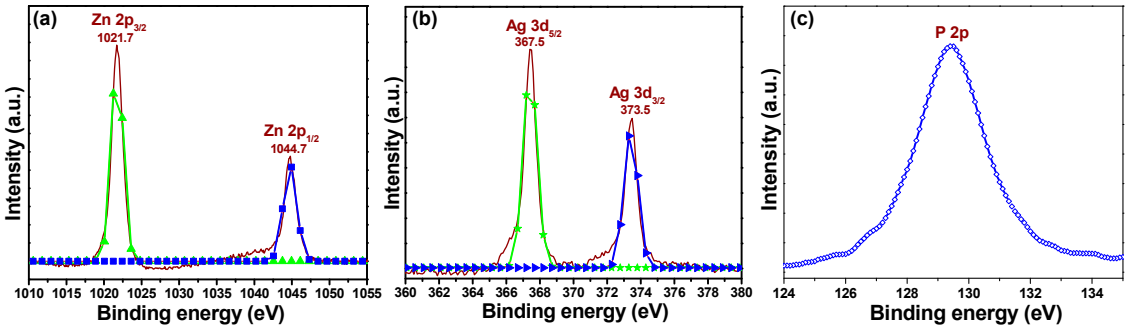

Figure 3. XPS binding energy spectra of the ZPBA nanocomposite. (**a**) Zn 2p peaks with its Gaussian-fitted components. (**b**) Ag 3d peaks with its Gaussian-fitted components. (**c**) P 2p core peaks.

3.2. Evaluation of Antibacterial Activity

The antibacterial activity of synthesized nanocomposites against type and TIG-R *A. baumannii* strains was assessed by determining MIC (Table 1). As shown in Table 1, the MIC values of BA, ZP and ZPB nanocomposites were >200 $\mu g \cdot mL^{-1}$ against all tested bacterial strains, indicating that BA, ZP and ZPB nanocomposites within this concentration range are not potential antibacterial agents. Meanwhile, ZPA against two strains (type and TIG-R) showed a >2-fold reduction in MIC. In particular, the TIG-R strain was more active against ZPA. As this effect is higher in the TIG-R strain than in the type strains, the role of Ag NP seems to enhance both the selectivity and activity of ZnO NP in killing bacteria. This increase was even much stronger in the case of ZPBA; the MIC ranged from 12.5 to 100 $\mu g \cdot mL^{-1}$, which showed a >2~4-fold increase in antibacterial activity compared to ZPA. In the case of ZPBA, the selective pressure to TIG-R was still retained, as in the ZPA, with similar efficiency assessed by a 2-fold difference in MIC between ZPA and ZPBA. Therefore, the ZPBA sample is a potent antibacterial agent against TIG-R *A. baumannii*.

It is noteworthy that the Ag NP in the ZPA sample was prepared from a surfactant-assisted approach, whereas the Ag NP in the ZPBA sample was synthesized using BP without additional surfactants. Therefore, the increased antibacterial activity of ZPBA nanocomposite can be attributed to the synergistic nature of the sample and the influence of BP. It is also worth mentioning the possible influence of BP on antibacterial activity by comparing the antibacterial activity of ZPBA (with BP) and ZPA (without BP), as both

samples showed antibacterial activity, but the presence of BP in the ZPBA sample not only helped in the formation of Ag NP (without any surfactant), but also helped in the antibacterial activity.

Table 1. Antibacterial activity of samples against *A. baumannii* strains [1].

Type of Bacteria	Strain Name [2]	MIC (μg·mL^{-1})				
		BA	ZP	ZPA	ZPB	ZPBA
Type	ATCC 19606	>200	>200	100	>200	25
Type	ATCC 15150	>200	>200	>200	>200	100
TIG-R	ATCC 19606-R	>200	>200	50	>200	12.5

[1] Values were obtained as previously described [33]. Data shown are representative of $n = 3$. [2] ATCC, American Type Culture Collection [www.atcc.org (accessed on 1 October 2023)]. Abbreviations: BA, BP-Ag; ZP, ZnO-PEG; ZPA, ZP-Ag; ZPB, ZP-BP; ZPBA, ZP-BP-Ag; MIC, Minimum inhibitory concentration; TIG-R, Tigecycline resistant *A. baumannii*.

3.3. Membrane Disruption and ROS Generation

The antibacterial mechanism of NPs or nanocomposites generally depends on their ability to disrupt the bacterial cell membrane, along with ROS production and are widely accepted antibacterial mechanisms to kill bacterial pathogens [41]. Hence, the possible antibacterial mechanism of the ZPBA nanocomposite was evaluated by SEM image analysis of the morphological changes in *A. baumannii* (Figure 4) after treatment with ZPBA. Compared to a smooth surface without membrane disruption of untreated *A. baumannii* cells (Figure 4a), ZPBA-treated *A. baumannii* cells (ATCC 19606) were more aggregated with a disrupted membrane structure (Figure 4b). The synergistic nature of the ZPBA nanocomposite can be attributed to its antibacterial potential, as BP [42], ZnO [43] and Ag [19] have their own membrane disruption ability. Since all the above materials are known to produce higher amounts of ROS species in bacterial killing as frequently reported [19,41], additionally, ROS production from different samples was measured against TIG-R (Figure 5). The results showed that all materials generated a higher amount of ROS than the control. As seen in Figure 5, the BP nanosheet or Ag incorporation into ZP retained ZP's ability to produce ROS. However, the ROS production from the ZPBA nanocomposite was less than that of the other nanocomposites. This result cannot warrant that the higher antibacterial activity of ZPBA compared to the other nanocomposites mainly originated from ROS generation. The above results suggest that the combined action of ZPBA by membrane disruption and ROS generation is a potential mechanism to kill bacterial cells, although the exact mechanism of ZPBA's selective action against TIG-R *A. baumannii* remains challenging.

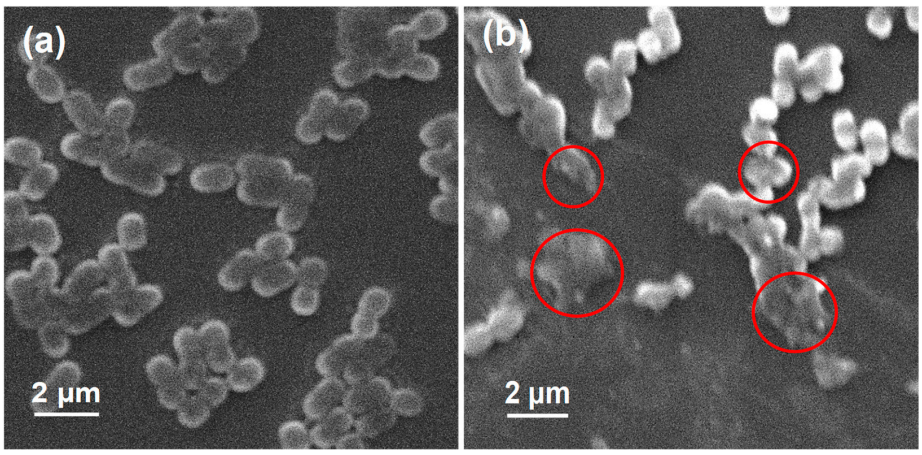

Figure 4. Scanning electron microscopy images of bacterial cells after various treatments. Untreated (**a**) *A. baumannii* (ATCC 19606) and (**b**) ZPBA-treated *A. baumannii* (ATCC 19606). Red circles indicate the disrupted regions of bacterial cells.

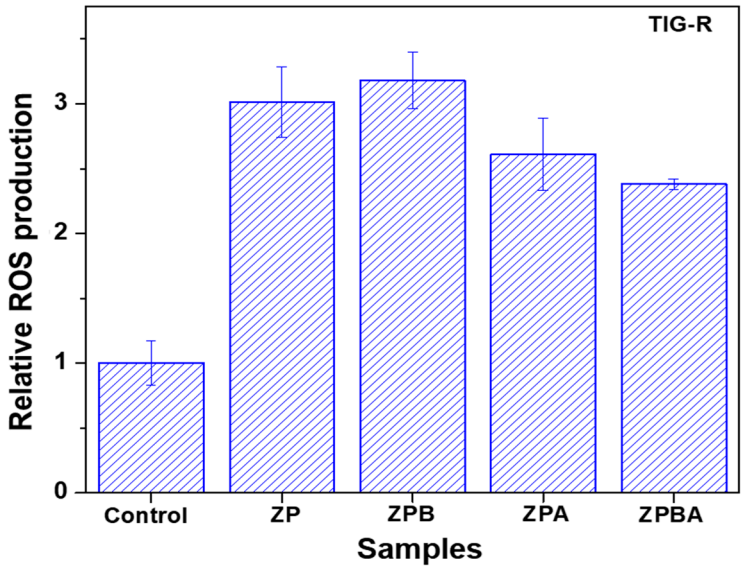

Figure 5. Reactive oxygen species (ROS)-mediated production of different samples against TIG-R. Fluorescence intensity at 520 nm of TIG-R cells treated with different samples was measured. PBS buffered reaction was used as a control. Three independent experiments were performed. The data were processed using MARS Data Analysis software (ver. 3.02 R2; BMG Labtech, Ortenberg, Germany). Relative ROS production by nanoparticles is shown from $n = 3$ ($p < 0.05$).

4. Conclusions

In this study, we synthesized ZnO and Ag NPs immobilized on BP NS, referred to as ZPBA, using a low-temperature solution process. ZPBA showed excellent potential for antibacterial activity against critically detrimental pathogens to human health, i.e., *A. baumannii* strains. In particular, ZPBA is better for an *A. baumannii* strain that is resistant to tigecycline, last-resort antibiotics against *A. baumannii* infection, resulting in bacterial death through the combination of membrane disruption and ROS generation mechanism. The BP in ZPBA acted as a green reductant to synthesize Ag NP without the addition of any surfactant. This work highlights the potential of Ag NP and BP NS as synergistic components in ZPBA nanocomposite action against the killing of *A. baumannii*, especially the TIG-R strains.

Supplementary Materials: The following supporting information can be downloaded at: https://www.mdpi.com/article/10.3390/jcs7100423/s1, Figure S1: XRD pattern of ZPA sample synthesized from surfactant-assisted approach; Figure S2: Minimum inhibitory concentrations (MICs) of ZP, ZP-BP (ZPB), ZP-Ag (ZPA), BP-Ag (BA) and ZP-BP-Ag (ZPBA) against *A. baumannii* (ATCC 19606). The MIC results from 96-well plates were photographed. Red circles indicate individual MIC values. Triplicate measurements are presented; Figure S3: Minimum inhibitory concentrations (MICs) of ZP, ZP-BP (ZPB), ZP-Ag (ZPA), BP-Ag (BA) and ZP-BP-Ag (ZPBA) against *A. baumannii* (ATCC 15150). The MIC results from 96-well plates were photographed. Red circles indicate individual MIC values. Triplicate measurements are presented; Figure S4: Minimum inhibitory concentrations (MICs) of ZP, ZP-BP (ZPB), ZP-Ag (ZPA), BP-Ag (BA) and ZP-BP-Ag (ZPBA) against TIG-R *A. baumannii*. The MIC results from 96-well plates were photographed. Red circles indicate individual MIC values. Triplicate measurements are presented.

Author Contributions: A.N.: Conceptualization, investigation, methodology, validation and writing—original draft; H.C.: Investigation, methodology and validation; K.-s.K.: Conceptualization, supervision, resources and writing—review & editing. All authors have read and agreed to the published version of the manuscript.

Funding: This research was financially supported by a National Research Foundation of Korea (NRF) grant funded by the Korean government (MSIT) (grant number NRF-2021R1A2C1007413) and the 2023 Post-Doc Development Program of Pusan National University.

Data Availability Statement: Not applicable.

Conflicts of Interest: The authors declare no conflict of interest.

References

1. Nocera, F.P.; Attili, A.R.; De Martino, L. Acinetobacter baumannii: Its Clinical Significance in Human and Veterinary Medicine. *Pathogens* **2021**, *10*, 127. [CrossRef] [PubMed]
2. WHO Publishes List of Bacteria for Which New Antibiotics Are Urgently Needed. Available online: https://www.who.int/news/item/27-02-2017-who-publishes-list-of-bacteria-for-which-new-antibiotics-are-urgently-needed (accessed on 1 October 2023).
3. Spellberg, B.; Rex, J.H. The value of single-pathogen antibacterial agents. *Nat. Rev. Drug Discov.* **2013**, *12*, 963. [CrossRef] [PubMed]
4. Piperaki, E.T.; Tzouvelekis, L.S.; Miriagou, V.; Daikos, G.L. Carbapenem-resistant *Acinetobacter baumannii*: In pursuit of an effective treatment. *Clin. Microbiol. Infect.* **2019**, *25*, 951–957. [CrossRef] [PubMed]
5. Stein, G.E.; Babinchak, T. Tigecycline: An update. *Diagn. Microbiol. Infect. Dis.* **2013**, *75*, 331–336. [CrossRef] [PubMed]
6. Jo, J.; Ko, K.S. Tigecycline Heteroresistance and Resistance Mechanism in Clinical Isolates of *Acinetobacter baumannii*. *Microbiol. Spectr.* **2021**, *9*, e0101021. [CrossRef]
7. Karakonstantis, S. A systematic review of implications, mechanisms, and stability of in vivo emergent resistance to colistin and tigecycline in *Acinetobacter baumannii*. *J. Chemother.* **2021**, *33*, 1–11. [CrossRef]
8. Ortega-Nieto, C.; Losada-Garcia, N.; Prodan, D.; Furtos, G.; Palomo, J.M. Recent Advances on the Design and Applications of Antimicrobial Nanomaterials. *Nanomaterials* **2023**, *13*, 2406. [CrossRef]
9. Gao, W.; Zhang, L. Nanomaterials arising amid antibiotic resistance. *Nat. Rev. Microbiol.* **2021**, *19*, 5–6. [CrossRef]
10. Mei, L.; Zhu, S.; Yin, W.; Chen, C.; Nie, G.; Gu, Z.; Zhao, Y. Two-dimensional nanomaterials beyond graphene for antibacterial applications: Current progress and future perspectives. *Theranostics* **2020**, *10*, 757–781. [CrossRef]
11. Zhang, C.; Wang, Y.; Ma, J.; Zhang., Q.; Wang., F.; Liu, X.; Xia, T. Black Phosphorus for Fighting Antibiotic-resistant Bacteria: What is known and what is missing. *Sci. Total. Environ.* **2020**, *721*, 137740. [CrossRef]
12. Guo, T.; Zhuang, S.; Qiu, H.; Guo, Y.; Wang, L.; Jin, G.; Lin, W.; Huang, G.; Yang, H. Black Phosphorus Nanosheets for Killing Bacteria through Nanoknife Effect. *Part. Part. Syst. Charact.* **2020**, *37*, 2000169. [CrossRef]
13. Naskar, A.; Lee, S.; Kim, K.-s. Au-ZnO Conjugated Black Phosphorus as a Near-Infrared Light-Triggering and Recurrence-Suppressing Nanoantibiotic Platform against *Staphylococcus aureus*. *Pharmaceutics* **2021**, *13*, 52. [CrossRef]
14. Cho, H.; Naskar, A.; Lee, S.; Kim, S.; Kim, K.-s. A New Surface Charge Neutralizing Nano-Adjuvant to Potentiate Polymyxins in Killing Mcr-1 Mediated Drug-Resistant *Escherichia coli*. *Pharmaceutics* **2021**, *13*, 250. [CrossRef]
15. Zhang, D.; Liu, H.M.; Shu, X.L.; Feng, J.; Yang, P.; Dong, P.; Xie, X.; Shi, Q. Nanocopper-loaded black phosphorus nanocomposites for efficient synergistic antibacterial application. *J. Hazard. Mater.* **2020**, *393*, 122317. [CrossRef]
16. Pardhi, D.M.; Şen Karaman, D.; Timonen, J.; Wu, W.; Zhang, Q.; Satija, S.; Mehta, M.; Charbe, N.; McCarron, P.A.; Tambuwala, M.M.; et al. Anti-bacterial activity of inorganic nanomaterials and their antimicrobial peptide conjugates against resistant and non-resistant pathogens. *Int. J. Pharm.* **2020**, *586*, 119531. [CrossRef]
17. Naskar, A.; Cho, H.; Kim, K.-s. Black phosphorus-based CuS nanoplatform: Near-infrared-responsive and reactive oxygen species-generating agent against environmental bacterial pathogens. *J. Environ. Chem. Eng.* **2022**, *10*, 108226. [CrossRef]
18. Benetti, G.; Cavaliere, E.; Banfi, F.; Gavioli, L. Antimicrobial Nanostructured Coatings: A Gas Phase Deposition and Magnetron Sputtering Perspective. *Materials* **2020**, *13*, 784. [CrossRef]
19. Ahmad, S.A.; Das, S.S.; Khatoon, A.; Ansari, M.T.; Afzal, M.; Hasnain, M.S.; Nayak, A.K. Bactericidal activity of silver nanoparticles: A mechanistic review. *Mater. Sci. Energy Technol.* **2020**, *3*, 756–769. [CrossRef]
20. Rai, M.; Yadav, A.; Gade, A. Silver nanoparticles as a new generation of antimicrobials. *Biotechnol. Adv.* **2009**, *27*, 76–83. [CrossRef]
21. Jin, J.-C.; Xu, Z.-Q.; Dong, P.; Lai, L.; Lan, J.-Y.; Jiang, F.-L.; Liu, Y. One-step synthesis of silver nanoparticles using carbon dots as reducing and stabilizing agents and their antibacterial mechanisms. *Carbon.* **2015**, *94*, 129–141. [CrossRef]
22. Meikle, T.G.; Dyett, B.P.; Strachan, J.B.; White, J.; Drummond, C.J.; Conn, C.E. Preparation, Characterization, and Antimicrobial Activity of Cubosome Encapsulated Metal Nanocrystals. *ACS Appl. Mater. Interfaces* **2020**, *12*, 6944–6954. [CrossRef] [PubMed]
23. More, P.R.; Pandit, S.; Filippis, A.; Franci, G.; Mijakovic, I.; Galdiero, M. Silver Nanoparticles: Bactericidal and Mechanistic Approach against Drug Resistant Pathogens. *Microorganisms* **2023**, *11*, 369. [CrossRef] [PubMed]
24. Alshameri, A.W.; Owais, M. Antibacterial and cytotoxic potency of the plant-mediated synthesis of metallic nanoparticles Ag NPs and ZnO NPs: A review. *OpenNano* **2022**, *8*, 100077. [CrossRef]
25. Bose, S.; Surendhiran, D.; Chun, B.S.; Arthanari, S.; Tran, V.N.; Lee, H.; Kang, H.W. Facile synthesis of black phosphorus-zinc oxide nanohybrids for antibacterial coating of titanium surface. *Colloids Surf. B Biointerfaces* **2022**, *219*, 112807. [CrossRef] [PubMed]
26. Baig, N.; Kammakakam, I.; Falath, W. Nanomaterials: A review of synthesis methods, properties, recent progress, and challenges. *Mater. Adv.* **2021**, *2*, 1821–1871. [CrossRef]
27. Bretos, I.; Jiménez, R.; Ricote, J.; Calzada, M.L. Low-temperature crystallization of solution-derived metal oxide thin films assisted by chemical processes. *Chem. Soc. Rev.* **2018**, *47*, 291–308. [CrossRef]

28. Benetti, G.; Cavaliere, E.; Canteri, A.; Landini, G.; Rossolini, G.M.; Pallecchi, L.; Chiodi, M.; Van Bael, M.J.; Winckelmans, N.; Bals, S.; et al. Direct synthesis of antimicrobial coatings based on tailored bi-elemental nanoparticles. *APL Mater.* **2017**, *5*, 036105. [CrossRef]
29. Benetti, G.; Cavaliere, E.; Brescia, R.; Salassi, S.; Ferrando, R.; Vantomme, A.; Pallecchi, L.; Pollini, S.; Boncompagni, S.; Fortuni, B.; et al. Tailored Ag-Cu-Mg multielemental nanoparticles for wide-spectrum antibacterial coating. *Nanoscale* **2019**, *11*, 1626–1635. [CrossRef]
30. Ouyang, J.; Liu, R.Y.; Chen, W.; Liu, Z.; Xu, Q.; Zeng, K.; Deng, L.; Shen, L.; Liu, Y.-N. A black phosphorus based synergistic antibacterial platform against drug resistant bacteria. *J. Mater. Chem. B* **2018**, *6*, 6302–6310. [CrossRef]
31. Naskar, A.; Lee, S.; Lee, Y.; Kim, S.; Kim, K.-s. A New Nano-Platform of Erythromycin Combined with Ag Nano-Particle ZnO Nano-Structure against Methicillin-Resistant *Staphylococcus aureus*. *Pharmaceutics* **2020**, *12*, 841. [CrossRef]
32. Cho, H.; Sondak, T.; Kim, K.-S. Characterization of increased extracellular vesicle-mediated tigecycline resistance in *Acinetobacter baumannii*. *Pharm.* **2023**, *15*, 1251. [CrossRef]
33. Naskar, A.; Shin, J.; Kim, K.-s. A MoS_2 based silver-doped ZnO nanocomposite and its antibacterial activity against β-lactamase expressing *Escherichia coli*. *RSC Adv.* **2022**, *12*, 7268–7275. [CrossRef] [PubMed]
34. Li, Q.; Ma, X.; Liu, H.; Chen, Z.; Chen, H.; Chu, S. Self-Organized Growth of Two-Dimensional GaTe Nanosheet on ZnO Nanowires for Heterojunctional Water Splitting Applications. *ACS Appl. Mater. Inter.* **2017**, *9*, 18836–18844. [CrossRef] [PubMed]
35. Zhu, L.; Li, H.; Liu, Z.; Xia, P.; Xie, Y.; Xiong, D. Synthesis of the 0D/3D CuO/ZnO Heterojunction with Enhanced Photocatalytic Activity. *J. Phys. Chem. C* **2018**, *122*, 9531–9539. [CrossRef]
36. Dai, L.; Strelow, C.; Kipp, T.; Mews, A.; Benkenstein, I.; Eifler, D.; Vuong, T.H.; Rabeah, J.; McGettrick, J.; Lesyuk, R.; et al. Colloidal Manganese-Doped ZnS Nanoplatelets and Their Optical Properties. *Chem. Mater.* **2021**, *33*, 275–284. [CrossRef]
37. Loka, C.; Lee, K.S. Enhanced Visible-Light-Driven Photocatalysis of Ag/Ag_2O/ZnO Nanocomposite Heterostructures. *Nanomaterials* **2022**, *12*, 2528. [CrossRef]
38. Li, W.; Li, K.; Ye, Y.; Zhang, S.; Liu, Y.; Wang, G.; Liang, C.; Zhang, H.; Zhao, H. Efficient electrocatalytic nitrogen reduction to ammonia with aqueous silver nanodots. *Commun. Chem.* **2021**, *4*, 10. [CrossRef]
39. Wu, Y.; Lin, Y.; Xu, J. Synthesis of Ag-Ho, Ag-Sm, Ag-Zn, Ag-Cu, Ag-Cs, Ag-Zr, Ag-Er, Ag-Y and Ag-Co metal organic nanoparticles for UV-Vis-NIR wide-range bio-tissue imaging. *Photochem. Photobiol. Sci.* **2019**, *18*, 1081–1091. [CrossRef]
40. Liao, J.; Xu, Y.; Zhao, Y.; Wang, C.-C.; Ge, C. Ag and Fe_3O_4 Comodified WO3—X Nanocomposites for Catalytic Photothermal Degradation of Pharmaceuticals and Personal Care Products. *ACS Appl. Nano Mater.* **2021**, *4*, 1898–1905. [CrossRef]
41. Godoy-Gallardo, M.; Eckhard, U.; Delgado, L.M.; de Roo Puente, Y.J.D.; Hoyos-Nogués, M.; Gil, F.J.; Perez, R.A. Antibacterial approaches in tissue engineering using metal ions and nanoparticles: From mechanisms to applications. *Bioact. Mater.* **2021**, *6*, 4470–4490. [CrossRef]
42. Phakatkar, A.H.; Firlar, E.; Alzate, L.; Song, B.; Narayanan, S.; Rojaee, R.; Foroozan, T.; Deivanayagam, R.; Banner, D.J.; Shahbazian-Yassar, R.; et al. TEM Studies on Antibacterial Mechanisms of Black Phosphorous Nanosheets. *Int. J. Nanomed.* **2020**, *15*, 3071–3085. [CrossRef] [PubMed]
43. Krishnamoorthy, R.; Athinarayanan, J.; Periyasamy, V.S.; Alshuniaber, M.A.; Alshammari, G.; Hakeem, M.J.; Ahmed, M.A.; Alshatwi, A.A. Antibacterial Mechanisms of Zinc Oxide Nanoparticle against Bacterial Food Pathogens Resistant to Beta-Lactam Antibiotics. *Molecules* **2022**, *27*, 2489. [CrossRef] [PubMed]